

REPORT

CHEMICAL PHYSICS

Quantum gas microscopy of Rydberg macrodimers

Simon Hollerith¹, Johannes Zeiher^{1*}, Jun Rui^{1†}, Antonio Rubio-Abadal¹, Valentin Walther², Thomas Pohl², Dan M. Stamper-Kurn³, Immanuel Bloch^{1,4}, Christian Gross¹

The subnanoscale size of typical diatomic molecules hinders direct optical access to their constituents. Rydberg macrodimers—bound states of two highly excited Rydberg atoms—feature interatomic distances easily exceeding optical wavelengths. We report the direct microscopic observation and detailed characterization of such molecules in a gas of ultracold rubidium atoms in an optical lattice. The bond length of about 0.7 micrometers, comparable to the size of small bacteria, matches the diagonal distance of the lattice. By exciting pairs in the initial two-dimensional atom array, we resolved more than 50 vibrational resonances. Using our spatially resolved detection, we observed the macrodimers by correlated atom loss and demonstrated control of the molecular alignment by the choice of the vibrational state. Our results allow for rigorous testing of Rydberg interaction potentials and highlight the potential of quantum gas microscopy for molecular physics.

A quantitative determination of the structure of molecules is an essential goal of physical chemistry and is crucial to revealing and understanding their properties. The high level of quantum control and the ultracold temperatures achieved in atomic physics provide tools to study molecules and their structure (1). Prominent examples include the observations of weakly bound Feshbach molecules (2, 3), the controlled photoassociation of individual molecules in a microtrap (4), molecules comprising ground-state atoms bound to a highly excited Rydberg atom (5–7), or pure long-range molecules (8, 9) that are bound purely electrostatically. The binding mechanism of the latter, where the electron orbitals of the constituents do not overlap, has also been predicted to pertain between two Rydberg atoms. These “Rydberg macrodimers” (10–14) are truly remarkable in their macroscopic bond lengths, which are 10,000 times those of usual diatomic molecules and thus reach typical interparticle distances in magneto-optical traps (15), optical lattices (16), or optical tweezers (17, 18). Their enormous size not only enables direct optical access to individual constituents, but also allows for the controlled binding of two atoms optically pinned at the correct distance. First signatures of Rydberg macrodimers have been observed in systems of laser-cooled atoms by spectroscopy (15) and pulsed-field ionization (19), but a vi-

brationally and spatially resolved detection has been lacking so far.

Here, we present a precise study of Rydberg macrodimers starting from ground-state ⁸⁷Rb atoms deterministically arranged in an optical lattice. We probed the vibrational levels by two-photon spectroscopy, resolving more than 50 excited vibrational resonances. The observed spectrum agrees quantitatively with ab initio calculations of Rydberg interaction potentials (20–22), providing a stringent test for their accuracy. Using the site-resolved detection and single-atom sensitivity of our quantum gas microscope (23, 24), we identified the macrodimer signal microscopically as a loss of pairs of ground-state atoms at a distance of a bond length. Furthermore, we controlled the spatial orientation of the photoassociated molecules by the parity of the vibrational wave function and the polarization of the excitation laser.

Rydberg interaction potentials are of van der Waals type for asymptotically large interatomic separations R (25), but the situation is more complicated at smaller distances. In a generic situation, repulsive interactions may increase the energy of a lower-lying pair state, $|\bar{\alpha}\rangle$, while attractive interactions decrease the energy of a higher-lying one, $|\beta\rangle$. At some specific distance, the two potentials become degenerate, and any finite coupling between them opens a gap (Fig. 1A), which is large when $|\bar{\alpha}\rangle$ and $|\beta\rangle$ contain large amplitudes of mutually dipole-dipole-coupled states. The resulting potential minimum hosts a series of bound macrodimer states $\Phi_{\nu}(R)$ (10, 11, 15), where ν denotes the vibrational quantum number of the nuclear motion. In our experiment, we chose such an avoided crossing of two 0_g^+ potentials with gerade symmetry and zero an-

gular momentum projection on the interatomic axis ($l, 20$). For large distances, the selected pair states transform into the states $|\bar{\alpha}\rangle \rightarrow |e, e\rangle \equiv |35P_{1/2}, 35P_{1/2}\rangle$ and $|\beta\rangle \rightarrow |e, e'\rangle \equiv |35P_{1/2}, 35P_{3/2}\rangle$ (26), which can be optically coupled from the ground state $|g, g\rangle$ by a two-photon transition. Here, $|g\rangle = |5S_{1/2} F = 2, m_F = 0\rangle$ and the bond length of this macrodimer state is predicted to be 720 nm, close to the diagonal lattice spacing of $R_{\text{in}} = 752$ nm in our optical lattice. With the atoms initially prepared in the motional ground state of the optical lattice, this coincidence of length scales results in a strong optical coupling due to the large wave function overlap.

Our experiments started with a two-dimensional atomic Mott insulator of ⁸⁷Rb with a lattice filling of $94 \pm 1\%$ in the atomic ground state. The atoms were pinned in a deep optical lattice with a root mean square (RMS) width $\sigma_{\text{lat}} = 68$ nm of the motional ground state in the atomic plane (Fig. 1B) with a temperature below the on-site trapping frequency. The molecules were photoassociated by an ultraviolet (UV) Rydberg excitation laser at a wavelength of 298 nm propagating along the diagonal direction of the optical lattice, with linear polarization aligned either in or orthogonal to the lattice plane. Our typical optical Rabi coupling from the state $|g\rangle$ to $|e\rangle$ was $\Omega/2\pi = 1.2 \pm 0.1$ MHz. We detected the excited macrodimers as missing pairs of ground-state atoms as these were ejected from the optical lattice very efficiently as a result of kinetic energy release in the macrodimer decay. The remaining ground-state atoms were then imaged with near-unity fidelity using a quantum gas microscope (Fig. 1D).

We first aimed to identify the presence of the bound macrodimers by their spectroscopic fingerprint. To this end, we illuminated the atomic ensemble for $t_{\text{UV}} = 100$ ms with the UV light polarized in the atomic plane for varying detuning Δ from the bare Rydberg state $|e\rangle$. In each step, we swept the optical frequency of the excitation laser by 480 kHz during the illumination time to ensure coverage of the full spectral region between neighboring data points. We observed the coupling to the bare Rydberg state $|e\rangle$ as a very broad saturated loss resonance (Fig. 2). At negative detunings, the resonance features an asymmetric broadening due to coupling to attractively interacting pair-state potentials (27). At positive detunings around $\Delta/2\pi = 180$ MHz, the first macrodimer bound state becomes two-photon resonant. A nonsaturated high-resolution spectrum of this line (Fig. 2C) features a full width at half maximum of 139 ± 5 kHz, which is of the same order as the measured linewidth of the bare Rydberg resonance (28). For higher vibrational resonances, we observed a reduction of the line strength, which we attribute to a combination of increased intermediate-state detuning and reduced overlap of the spatial wave functions. In addition, we observed a suppression of the excitation to odd vibrational states ν due to the approximate odd parity symmetry of the molecular wave functions with respect to the equilibrium distance. This is consistent with the Franck-Condon principle, which predicts the coupling

¹Max-Planck-Institut für Quantenoptik, 85748 Garching, Germany. ²Department of Physics and Astronomy, Aarhus University, DK 8000 Aarhus C, Denmark. ³Department of Physics, University of California, Berkeley, CA 94720, USA.

⁴Fakultät für Physik, Ludwig-Maximilians-Universität München, 80799 München, Germany.

*Present address: Department of Physics, University of California, Berkeley, CA 94720, USA.

†Corresponding author. Email: jun.rui@mpq.mpg.de

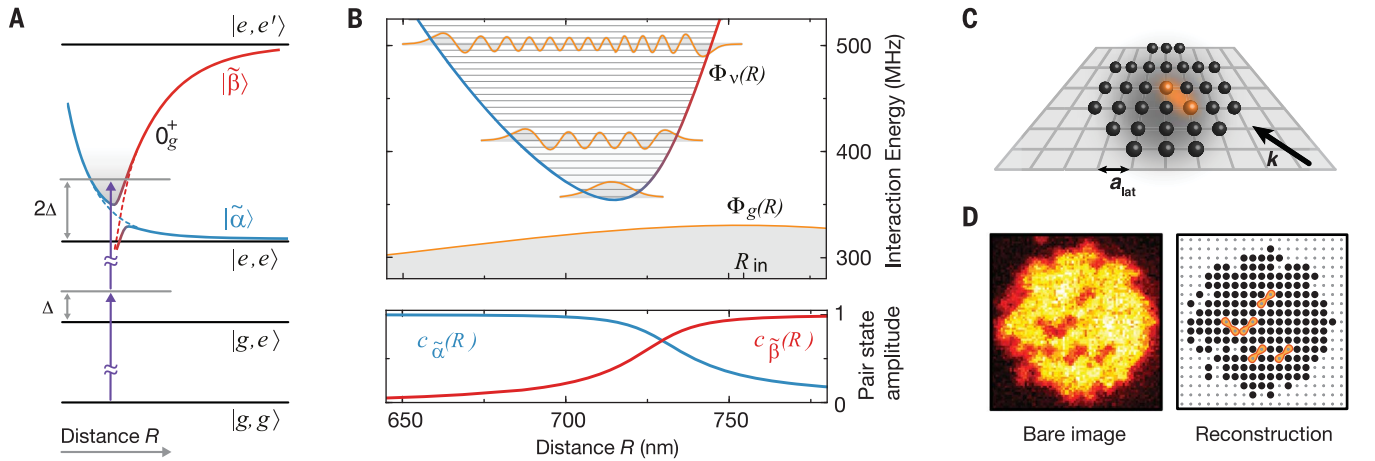


Fig. 1. Schematic of the experiment. (A) The two-photon and two-atom excitation from the ground state $|g, g\rangle$ occurs off-resonantly with detuning Δ via intermediate states where one atom is excited to the Rydberg state $|e\rangle \equiv |35P_{1/2}\rangle$. The avoided crossing of two coupled Rydberg interaction potentials $|\tilde{\alpha}\rangle$ and $|\tilde{\beta}\rangle$ (blue and red solid lines) leads to the formation of a binding potential, whose molecular states can be laser-excited if 2Δ matches the interaction shift from the asymptotic pair state $|e, e\rangle$. (B) The potential well hosts bound states (gray horizontal lines) with an energy spacing of ~ 6 MHz. The vibrational wave functions, indicated in orange, are

much narrower in the internuclear distance R than the RMS width of $\sqrt{2}\sigma_{\text{lat}}$ of the initial relative wave packet $\Phi_g(R)$ in the lattice. The lower panel shows the amplitudes $c_{\tilde{\alpha}, \tilde{\beta}}(R)$ resulting from a spatially dependent decomposition of the binding potential. (C) The atoms are initially arranged in a regular grid of lattice sites with a lattice constant $a_{\text{lat}} = 532$ nm and illuminated by the UV laser with wave vector k . (D) An exemplary fluorescence image of an atomic cloud illustrates the correlated losses due to molecule formation (left), indicated as orange symbols in the reconstructed image (right).

to be proportional to the overlap integrals of the broad initial and the tightly confined final spatial wave functions $\Phi_g(R)$ and $\Phi_v(R)$ (Fig. 1B). However, a closer inspection of the experimental data shows that this simple picture needs to be refined. Repeating the spectroscopy with orthogonal polarization (so that the optical electric field oscillates out of the atomic plane) results in a suppression of the line strength of the even lines.

Our microscopic access provides direct in situ information about the spatial alignment of the associated molecules and valuable insights into the underlying coupling mechanism (26, 29, 30). We compared different molecular lines by illuminating the cloud with UV light, resonant with a given vibrational state v , until the filling of the lattice decreased to roughly $87 \pm 1\%$. For a quantitative analysis, we evaluated spatially averaged density-density correlations $g^{(2)}(i, j) = \langle \langle \hat{n}_{k+i, l+j} \hat{n}_{k, l} \rangle - \langle \hat{n}_{k+i, l+j} \rangle \langle \hat{n}_{k, l} \rangle \rangle_{k, l}$ for the measured spatial atom distributions on a region of interest of 9×9 lattice sites (Fig. 3). Correlations show a clear peak at a distance of a lattice diagonal, revealing the bond length of the molecule. Moreover, we controlled the orientation of the photoassociated molecules by choosing a combination of vibrational quantum number and polarization of the light field. For even oscillator states v , the correlations are stronger along the lattice diagonal parallel to the polarization of the excitation light. The molecular orientation, however, flips when considering odd oscillator states for which the dimers form predominantly along the direction perpendicular to the polarization.

The key to understanding this striking alternation in the orientation of the molecules is the interplay of electronic and motional degrees of freedom. The Born-Oppenheimer wave function

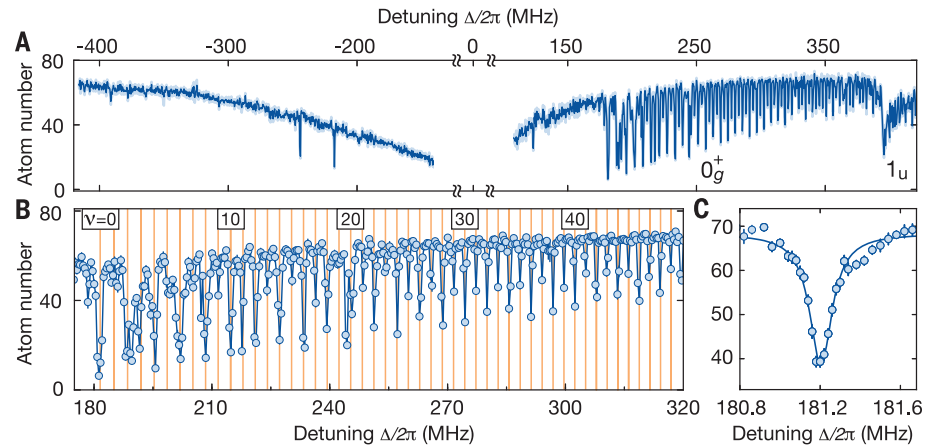


Fig. 2. High-resolution spectroscopy detuned from the Rydberg resonance. (A) Wide-range spectroscopy signal. We find no signatures of bound states on the interaction-broadened red-detuned side of the Rydberg resonance [the two isolated features are due to lattice-induced Raman resonances (26)]. On the blue-detuned side, we observe clear dips with regular spacing and alternating line strength due to the coupling to macrodimers. For very large detuning, a second series of molecular bound states belonging to a 1_u potential becomes resonant. (B) Zooming into the frequency region between 180 and 320 MHz reveals a spacing of the vibrational resonances of ~ 3 MHz, which slightly decreases for higher vibrational states. We find very good agreement with the theoretical predictions (orange lines), but the line strengths are saturated in the experiment (see fig. S8 for a nonsaturated measurement). (C) High-resolution spectroscopy of the lowest vibrational level. Error bars denote SEM.

of the macrodimer can be expressed as $|\Psi_{\text{Mol}}^v(R)\rangle = \Phi_v(R)|\chi_{\text{el}}(R)\rangle$. Whereas at large distances, the electronic part $|\chi_{\text{el}}(R)\rangle = c_{\tilde{\alpha}}(R)|\tilde{\alpha}\rangle + c_{\tilde{\beta}}(R)|\tilde{\beta}\rangle$ (11, 12) is dominated by the state $|\tilde{\beta}\rangle$, for short distances the $|\tilde{\alpha}\rangle$ contribution dominates (Fig. 1B), and this parametric dependence of the electronic potential has to be taken into account in the optical excitation. The two-photon Rabi coupling

$\tilde{\Omega}_v$ from the ground state to the macrodimer states thus splits into two terms. Neglecting the weak spatial dependence of the two-photon Rabi couplings $\tilde{\Omega}_{\tilde{\alpha}}(\tilde{\Omega}_{\tilde{\beta}})$ to the states $|\tilde{\alpha}\rangle(|\tilde{\beta}\rangle)$, we obtain $\tilde{\Omega}_v \approx \tilde{\Omega}_{\tilde{\alpha}} f_{\tilde{\alpha}}^v + \tilde{\Omega}_{\tilde{\beta}} f_{\tilde{\beta}}^v$ with the generalized Franck-Condon integrals $f_{\tilde{\alpha}}^v = \int \Phi_v^*(R) c_{\tilde{\alpha}}^*(R) \Phi_g(R) dR$ and $f_{\tilde{\beta}}^v$ (26, 29). Because of the change of the pair state amplitudes around the potential minimum

(Fig. 1B), $f_{\tilde{\alpha}}^v$ and $f_{\tilde{\beta}}^v$ have the same sign for even v but an opposite sign for odd v . The electronic contributions $\tilde{\Omega}_{\tilde{\alpha}}$ ($\tilde{\Omega}_{\tilde{\beta}}$) depend on the alignment of the polarization relative to the molecular axis because the states $|\tilde{\alpha}\rangle$ ($|\tilde{\beta}\rangle$) obey molecular symmetry constraints. In the case where the axes are parallel, $\tilde{\Omega}_{\tilde{\alpha}}$ and $\tilde{\Omega}_{\tilde{\beta}}$ have the same sign and therefore both terms in $\tilde{\Omega}_v$ add constructively for even vibrational states, leading to a dominating signal in $g^{(2)}(1, 1)$. For the perpendicular case, the sign of $\tilde{\Omega}_{\tilde{\beta}}$ flips and constructive interference occurs for odd vibrational states, resulting in a stronger value for $g^{(2)}(1, -1)$. Moreover, for the measurement with light polarized out of plane (Fig. 1A), the spatial signal exhibits isotropic correlations because in that case the polarization is perpendicular to both lattice diagonals.

Although most of the line positions of the measured spectrum shown in Fig. 2 agree with

the theoretical model, we find deviations for low-lying oscillator states. A finer scan of that region is shown in Fig. 4A. These deviations originate from a third pair state $|\tilde{\gamma}\rangle$ asymptotically corresponding to the optically uncoupled state $|32D_{3/2}, 37P_{1/2}\rangle$ intersecting the binding potential around the potential minimum. At the degeneracy point, the weak dipole-quadrupole coupling between the intersecting potentials opens another gap energetically comparable to the vibrational energy. As a consequence, a separation of the vibrational motion and interatomic interaction is no longer possible. For the theory used to describe the coarse vibrational structure shown in Fig. 2, we only accounted for the crossing formed by the coupling between $|\tilde{\alpha}\rangle$ and $|\tilde{\beta}\rangle$. We extended our theory by allowing for the vibronic coupling between the vibrational modes and the electronic states $|\tilde{\alpha}\rangle$, $|\tilde{\beta}\rangle$, and $|\tilde{\gamma}\rangle$.

The modified eigenenergies are indicated as orange lines in Fig. 4B. Using the refined theory, we indeed can identify almost all observed lines. To confirm the effect of the intersection, we repeated our spectroscopic measurements for the lowest states in the analogous potential for $n = 36$, where such an additional crossing is absent. In this case, we observed a pure harmonic oscillator-like spectrum in excellent agreement with the calculations. The remarkably high sensitivity of the measured line structure to even weak modifications of the interaction potentials underlines the promise of Rydberg macrodimer spectroscopy for benchmarking Rydberg interaction potentials. This also holds for Rydberg interactions in the presence of applied magnetic fields, where accurate calculations are more difficult (26).

In the future, the coupling to macrodimers could be used to realize quantum gates at well-defined qubit distance or to enhance Rydberg dressing schemes (28, 31), where the pair state admixture of the strongly interacting doubly excited state is enhanced relative to the singly excited intermediate states. The strongly spatially dependent loss revealed in the correlation measurements and also by modulating the initial atom distribution (26) could be used to engineer dissipatively stabilized few- or many-body states (32, 33). Furthermore, the approach demonstrated here can readily be extended to study multi-atom bound states (34, 35). Finally, bringing the coupling rate to the macrodimers closer to the decay rate of the individual Rydberg atoms may allow for the observation of novel many-body physics arising from spatial constraints and coherent interactions.

Fig. 3. Macrodimers imaging and molecular orientation on the lattice.

(A) Evaluating $g^{(2)}(i, j)$ after illuminating the atoms with UV light polarized in the atomic plane for various macrodimer lines v reveals a directionality in the excitation rate. For even vibrational

states, the excitation rate is stronger along the polarization of the excitation laser, whereas odd states favor molecule formation perpendicular to the polarization. For both cases, we show an exemplary image from our microscope. The origin of the alternating molecular orientation is the polarization of the light with respect to the quantization axis of the dimer. The light is π -polarized with both axes aligned and σ^+ -polarized in the perpendicular case. (B) For out-of-plane polarization, there is no longer a preferred direction and we observe equal correlations for both diagonal directions.

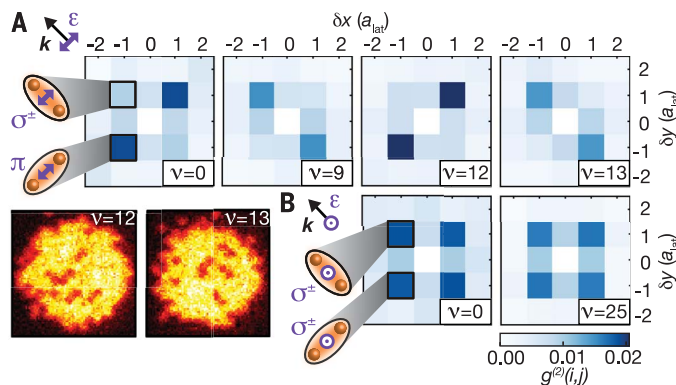
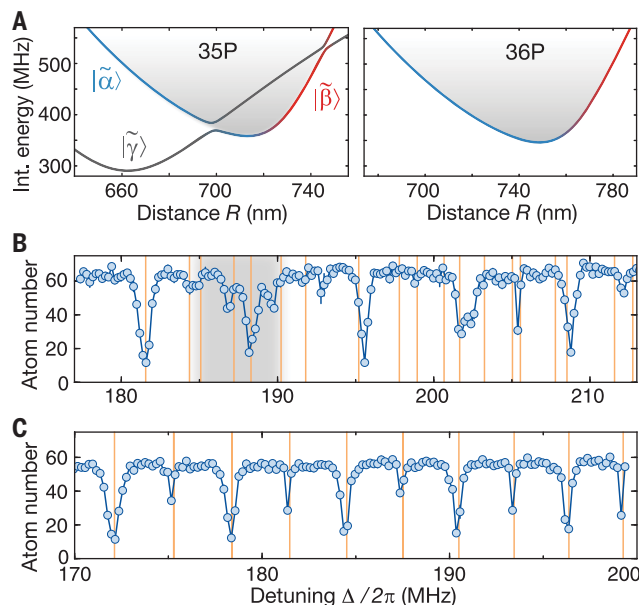


Fig. 4. Breakdown of the Born-Oppenheimer approximation.

(A) A closer look at the potential for $n = 35$ reveals a 12-MHz-wide gap, which is absent for $n = 36$. (B) We find a modification of the coarse spectrum discussed in Fig. 2B in the vicinity of the gap (gray shaded region). A theoretical treatment including the gap (orange lines) allows for an assignment of most of the observed lines. (C) For $n = 36$, the measured spectrum agrees well with the theoretical expectation. The excitation light was polarized in the atomic plane; error bars denote SEM.



REFERENCES AND NOTES

1. K. M. Jones, E. Tiesinga, P. D. Lett, P. S. Julienne, *Rev. Mod. Phys.* **78**, 483–535 (2006).
2. C. A. Regal, C. Ticknor, J. L. Bohn, D. S. Jin, *Nature* **424**, 47–50 (2003).
3. S. A. Moses et al., *Science* **350**, 659–662 (2015).
4. L. R. Liu et al., *Science* **360**, 900–903 (2018).
5. T. F. Gallagher, *Rydberg Atoms* (Cambridge Univ. Press, 1994).
6. V. Bendkowsky et al., *Nature* **458**, 1005–1008 (2009).
7. J. P. Shaffer, S. T. Rittenhouse, H. R. Sadeghpour, *Nat. Commun.* **9**, 1965 (2018).
8. J. D. Miller, R. A. Cline, D. J. Heinzen, *Phys. Rev. Lett.* **71**, 2204–2207 (1993).
9. P. D. Lett et al., *Phys. Rev. Lett.* **71**, 2200–2203 (1993).
10. C. Boisseau, I. Simbotin, R. Côté, *Phys. Rev. Lett.* **88**, 133004 (2002).
11. J. Stanojevic et al., *Eur. Phys. J. D* **40**, 3–12 (2006).
12. J. Stanojevic, R. Côté, D. Tong, E. E. Eyler, P. L. Gould, *Phys. Rev. A* **78**, 052709 (2008).
13. A. Schwettmann, J. Crawford, K. R. Overstreet, J. P. Shaffer, *Phys. Rev. A* **74**, 020701 (2006).
14. A. Schwettmann, K. R. Overstreet, J. Tallant, J. P. Shaffer, *J. Mod. Opt.* **54**, 2551–2562 (2007).
15. H. Saßmannshausen, J. Deiglmayr, *Phys. Rev. Lett.* **117**, 083401 (2016).
16. E. Guardado-Sanchez et al., *Phys. Rev. X* **8**, 021069 (2018).
17. H. Bernien et al., *Nature* **551**, 579–584 (2017).
18. H. Labuhn et al., *Nature* **534**, 667–670 (2016).
19. K. R. Overstreet, A. Schwettmann, J. Tallant, D. Booth, J. P. Shaffer, *Nat. Phys.* **5**, 581–585 (2009).
20. S. Weber et al., *J. Phys. B* **50**, 133001 (2017).
21. N. Šibalić, J. D. Pritchard, C. S. Adams, K. J. Weatherill, *Comput. Phys. Commun.* **220**, 319 (2017).
22. J. Deiglmayr, *Phys. Scr.* **91**, 104007 (2016).
23. J. F. Sherson et al., *Nature* **467**, 68–72 (2010).
24. W. S. Bakr et al., *Science* **329**, 547–550 (2010).
25. M. Saffman, T. G. Walker, K. Molmer, *Rev. Mod. Phys.* **82**, 2313–2363 (2010).

26. See supplementary materials.
27. K. Singer, M. Reetz-Lamour, T. Amthor, L. G. Marcassa, M. Weidemüller, *Phys. Rev. Lett.* **93**, 163001 (2004).
28. J. Zeiher *et al.*, *Nat. Phys.* **12**, 1095–1099 (2016).
29. N. Samboy, R. Côté, *J. Phys. B* **44**, 184006 (2011).
30. N. Samboy, J. Stanojevic, R. Côté, *Phys. Rev. A* **83**, 050501 (2011).
31. R. M. W. van Bijnen, T. Pohl, *Phys. Rev. Lett.* **114**, 243002 (2015).
32. C. Ates, B. Olmos, W. Li, I. Lesanovsky, *Phys. Rev. Lett.* **109**, 233003 (2012).
33. N. Syassen *et al.*, *Science* **320**, 1329–1331 (2008).
34. N. Samboy, R. Côté, *Phys. Rev. A* **87**, 032512 (2013).
35. M. Kiffner, W. Li, D. Jaksch, *Phys. Rev. Lett.* **111**, 233003 (2013).
36. The data displayed in the figures of this manuscript are available from the Edmond repository of the Max Planck Society, doi 10.17617/3.29.

ACKNOWLEDGMENTS

We thank all contributors to the open-source programs “pair interaction” and “ARC” as well as R. Côté, W. D. Phillips, N. Šibalić, and J. Deiglmayr for valuable discussions. **Funding:** We acknowledge support by the DNRF through a Niels Bohr Professorship for T.P. and funding by MPG. This project has received funding from the European Union’s Horizon 2020 research and innovation program under grant agreement 817482 (PASQuanS) and the European Research Council (ERC) 678580 (RyD-QMB) and also from project 319278 (UQUAM) of the Seventh Framework Programme. We also acknowledge funding from Deutsche Forschungsgemeinschaft (project BL 574/15-1) within SPP 1929 (GiRyd). **Author contributions:** S.H. and J.R. acquired the data underlying this study and, together with J.Z. and A.R.-A., they maintained and improved the experimental setup. V.W. and T.P. contributed the theoretical predictions. I.B. and C.G.

supervised the study. All authors worked on the interpretation of the data and contributed to the final manuscript. **Competing interests:** The authors declare no competing interests. **Data and materials availability:** The data that support the plots presented in this paper are publicly available from the Open Access Data Repository of the Max Planck Society (36).

SUPPLEMENTARY MATERIALS

science.sciencemag.org/content/364/6441/664/suppl/DC1
Materials and Methods
Figs. S1 to S9
Tables S1 and S2
References (37–41)

18 December 2018; accepted 18 April 2019
10.1126/science.aaw4150

Quantum gas microscopy of Rydberg macrodimers

Simon Hollerith, Johannes Zeiher, Jun Rui, Antonio Rubio-Abadal, Valentin Walther, Thomas Pohl, Dan M. Stamper-Kurn, Immanuel Bloch and Christian Gross

Science **364** (6441), 664-667.
DOI: 10.1126/science.aaw4150

Bonding's outer limit

In a Rydberg state, an atom has been very nearly, but not quite, ionized. This puts the electron relatively far from the nucleus, and two atoms in such a state can thus form a rather long-range bond. Hollerith *et al.* observed this phenomenon in fine detail by exciting pairs of ultracold rubidium atoms along the diagonal of an optical lattice. The authors resolved the vibrational state structure spectroscopically and showed that the Rydberg dimers manifested bond lengths exceeding 700 nanometers.

Science, this issue p. 664

ARTICLE TOOLS

<http://science.sciencemag.org/content/364/6441/664>

SUPPLEMENTARY MATERIALS

<http://science.sciencemag.org/content/suppl/2019/05/15/364.6441.664.DC1>

REFERENCES

This article cites 39 articles, 4 of which you can access for free
<http://science.sciencemag.org/content/364/6441/664#BIBL>

PERMISSIONS

<http://www.sciencemag.org/help/reprints-and-permissions>

Use of this article is subject to the [Terms of Service](#)